Author Manuscript

Author Manuscript

Author Manuscript

Author Manuscript

HHS Public Access

Author manuscript

Nat Cell Biol. Author manuscript; available in PMC 2018 January 22.

Published in final edited form as:

Nat Cell Biol. 2017 May ; 19(5): 542–549. doi:10.1038/ncb3510.

A three-dimensional model of human lung development and disease from pluripotent stem cells

Ya-Wen Chen[1,2,3], **Sarah Xuelian Huang**[1,2,3], **Ana Luisa Rodrigues Toste de Carvalho**[1,2,3,4,5], **Siu-Hong Ho**[2,3], **Mohammad Naimul Islam**[3], **Stefano Volpi**[6,7], **Luigi D Notarangelo**[6], **Michael Ciancanelli**[8], **Jean-Laurent Casanova**[8], **Jahar Bhattacharya**[3,12], **Alice F. Liang**[9], **Laura M Palermo**[10,13], **Matteo Porotto**[10,13], **Anne Moscona**[10,11,12,13], and **Hans-Willem Snoeck**[1,2,3,11,14]

[1]Columbia Center for Human Development, Columbia University Medical Center, New York, NY 10032, USA

[2]Columbia Center for Translational Immunology, Columbia University Medical Center, New York, NY 10032, USA

[3]Department of Medicine, Columbia University Medical Center, New York, NY 10032, USA

[4]Life and Health Sciences Research Institute (ICVS), School of Health Sciences, University of Minho, 4710-057 Braga, Portugal

[5]ICVS/3B's, PT Government Associate Laboratory, 4710-057 Braga/Guimarães, Portugal

[6]Division of Immunology and Manton Center for Orphan Disease Research, Children's Hospital, Harvard Medical School, Boston, MA 02115, USA

[7]U.O. Pediatria 2, Istituto Giannina Gaslini, Genoa, Italy

[8]St. Giles Laboratory of Human Genetics of Infectious Diseases, Rockefeller Branch, The Rockefeller University, New York, NY 10065, USA

[9]OCS Microscopy Core, New York University Langone Medical Center, New York, NY 10016

[10]Department of Pediatrics, Columbia University Medical Center, New York, NY 10032, USA

[11]Department of Microbiology and Immunology, Columbia University Medical Center, New York, NY 10032, USA

[12]Department of Physiology & Cellular Biophysics, Columbia University Medical Center, New York, NY 10032, USA

Users may view, print, copy, and download text and data-mine the content in such documents, for the purposes of academic research, subject always to the full Conditions of use: http://www.nature.com/authors/editorial_policies/license.html#terms

[14]Correspondence should be addressed to H.W.S hs2680@columbia.edu.

Authors Contributions

YWC designed and performed most experiments, contributed to the concept, and co-wrote the manuscript with HWS. SXH and ALRT assisted YWC. AFL performed transmission electron microscopy. SHH provided assistance with flow cytometry. JLC and MC provided patient material, and LN and SV generated the C12 IRF7-deficient iPS line. MNI and JB provided SFTPB-BODIPY. AM, MP and LMP generated and provided virology reagents, and provided design and instruction for experiments involving RSV. HWS provided concept and guidance, and co-wrote with YWC.

Competing Financial Interests

The authors have no competing financial interests.

Author Manuscript Author Manuscript Author Manuscript Author Manuscript

[13]Center for Host-Pathogen Interaction, Columbia University Medical Center, New York, NY 10032, USA

Abstract

Recapitulation of lung development from human pluripotent stem cells (hPSCs) in three dimensions (3D) would allow deeper insight into human development, as well as the development of innovative strategies for disease modeling, drug discovery and regenerative medicine[1]. We report here the generation from hPSCs of lung bud organoids (LBOs) that contain mesoderm and pulmonary endoderm and develop into branching airway and early alveolar structures after xenotransplantation and in Matrigel 3D culture. Expression analysis and structural features indicated that the branching structures reached the second trimester of human gestation. Infection *in vitro* with respiratory syncytial virus, which causes small airway obstruction and bronchiolitis in infants[2], led to swelling, detachment and shedding of infected cells into the organoid lumens, similar to what has been observed in human lungs[3]. Introduction of mutation in HPS1, which causes an early-onset form of intractable pulmonary fibrosis[4,5], led to accumulation of extracellular matrix and mesenchymal cells, suggesting the potential use of this model to recapitulate fibrotic lung disease *in vitro*. LBOs therefore recapitulate lung development and may provide a useful tool to model lung disease.

The respiratory system originates from buds that arise on the ventral aspect of the anterior foregut endoderm (AFE) and develop through a stereotyped branching process into proximal airways and distal alveolar progenitors (pseudoglandular stage). During the canalicular stage, cell cycle activity decreases, and specialization of the airway epithelium occurs in the stalks, with the emergence of basal, goblet, club, ciliated, and other cell types. This stage is followed by the saccular stage, where the canaliculi widen into distal sacculations that will give rise to primitive alveoli[6,7]. Organoids are *in vitro* generated 3D structures containing multiple cell types that are organized similar to an organ and recapitulate some specific organ function[1]. One group reported generation of human lung organoids[8,9]. However, while these small structures contained cells expressing markers of lung and airway[8] and have some airway potential after subcutaneous xenografting in mice[9], they do not satisfy the aforementioned criteria for organoids, as neither features of lung development, notably branching morphogenesis and proximodistal specification, nor function were observed.

We previously reported a strategy to differentiate hPSCs (embryonic stem cells (ESCs) and induced pluripotent stem cells (iPSCs)) in 2D through sequential developmental steps from definitive endoderm (DE) to AFE, lung field progenitors, and, finally, lung and airway epithelial cells (Supplementary Fig. 1a)[10–12]. Early during induction of a ventral lung fate from AFE adherent structures formed that detached easily and expanded in suspension culture as clumps of cells (Fig. 1a,b) in the presence of BMP4, FGF10, FGF7, retinoic acid (RA) and the GSK3β antagonist, CHIR99201 (Supplementary Fig. 1b), factors shown previously to be required for lung development[6,7]. 7.5×10^5 DE cells yielded 2490±129 clumps (n=3; RUES2 ESCs). The structures formed folding sheets of EPCAM $^+$KRT8$^+$ECAD$^+$FOXA1/2$^+$ AFE cells (FOXA2: 89.07% ± 3.36%, EPCAM+: 92.08% ± 1.88%, n=3; RUES2 ESCs) (Fig. 1c). By d25 51.26±4.37% (n=3; RUES2 ESCs) of the cells expressed the lung marker NKX2.1$^+$ (Fig. 1c). Except for the epithelial progenitor

Author Manuscript Author Manuscript Author Manuscript Author Manuscript

marker, p63 (18.59% ± 1.49%, n=3; RUES2 ESCs, Fig. 1c), markers of mature lung and airway cells were absent (not shown). The cells were surrounded by mesodermal PDGFRA $^{+}$ECAD^{-} cells (Fig. 1d). RNAseq (Supplementary Fig. 1c) confirmed strong enrichment of endoderm/lung genes (FOXA2, SOX2, NKX2.1) in EPCAM^{+} cells (Fig. 1e). EPCAM^{-} cells expressed mesodermal genes (Fig. 1e), some of which, such as TBX4 and HOX5 paralogs, are expressed in pulmonary mesoderm[13,14]. Genes expressed in mature lung and airway and in other AFE-derived lineages were nearly undetectable in the EPCAM^{+} fraction (Supplementary Fig. 1d). Sonic Hedgehog (SHH) was expressed in endodermal cells, and its transcriptional targets[15], PTCH1, GLI1 and HHIP in mesoderm (Supplementary Fig. 1d). In situ hybridization confirmed SHH expression in the endodermal fraction at d15. At d25, SHH was expressed most strongly in the tips of budding epithelial structures (Supplementary Fig. 1e). These findings are consistent with the developing mouse lung where SHH is expressed throughout the pulmonary endoderm early but is limited to branch tips during branching morphogenesis[15–17]. Because they contain multiple cell types that are spatially organized similar to developing lung buds *in vivo*, we call these structures lung bud organoids (LBOs).

When transplanted under the kidney capsule of immunodeficient NSG mice, LBOs yielded growths (Fig. 2a) containing tubular structures surrounded by mesenchymal tissue after 1.5 months (Fig. 2b). The tubes were uniformly lined by a FOXA2^{+}NKX2.1^{+}SOX2^{+} epithelium containing MUC5AC^{+} (goblet) cells with p63^{+} cells in the basal layer (Fig. 2c), compatible with airway epithelium. All cells were human (Supplementary Fig. 2a), except for endothelial cells, which were of mouse origin (Supplementary Fig. 2b). After 5 months, branching structures (Fig. 2d, Supplementary Fig. 2c) surrounded by SMA^{+} mesodermal cells arose (Supplementary Fig. 2c). All epithelial cells were NKX2.1^{+} while SOX2, a proximal marker later in lung development[18,19], was excluded from the branch tips, which expressed SFTPB and SFTPC, markers of surfactant-producing type II alveolar epithelial (ATII) cells (Fig. 2e)[20]. The stalks and central tubules expressed the proximal (airway) markers FOXJ1 (ciliated cells), CC10 (club cells) and mucins (goblet cells) (Fig. 2e). Hematoxylin-eosin staining showed abundant multiciliated cells (Supplementary Fig. 2d), while live imaging documented beating cilia (Supplementary Video 1). Furthermore, submucosal glands were observed near the larger tubular structures (Supplementary Fig. 2e). Overall, morphology and expression pattern within the growths are consistent with proximodistal specification during lung branching morphogenesis[6,7]. The fluid in the tubular structures contained all tested secretory products of lung and airway but was negative for the cell surface mucin[21], MUC1, indicating detection of secreted proteins and not proteins associated with sloughed cells, and providing evidence for function (Fig. 2f). After 7 months, dome-shaped groups of CGRP^{+}PGP9.5^{+} cells, compatible with neuroepithelial bodies[22], were present in the airway-like structures (Fig. 2g). Furthermore, areas of the growths developed into a network of thin cell layers (Fig. 2g) containing cells expressing ATII cells markers (SFTPC, ABCA3, HT2-280)[23] and cells bearing type I alveolar epithelial cell (ATI) markers (HT1-56, HOPX, PDPN, CAV1, SCNN1A, AKAP5, CLIC5)[20], although other markers for mature ATI cells (RAGE, AQP5)[20] were not detected (Fig. 2g). An alveolar capillary network and bronchoalveolar ducts were not observed, however. We conclude that, although full phenotypic and architectural alveolar maturation was not

Author Manuscript Author Manuscript Author Manuscript Author Manuscript

achieved, possibly at least in part because of the ectopic location, LBOs recapitulate many essential features of lung development, including branching morphogenesis and proximodistal specification, after xenotransplantation.

After embedding d25 LBOs in Matrigel in the presence of CHIR99021, FGF10, FGF7, BMP4 and RA (Supplementary Fig. 1b), >95% yielded rapidly expanding branching structures (Fig. 3a, Supplementary Fig. 3a for iPSCs, including C12, a line from a patient with mutations IRF7, causing acute respiratory distress syndrome after influenza infection)[24] expressing markers of pulmonary endoderm ($FOXA2^+$: 95.17%±1.54%, $NKX2.1^+$: 74.97%± 4.37%, $EPCAM^+$: 96.83% ± 0.62%, $SOX9^+$: 92.42% ± 3.81% n=3 at d70; RUES2 ESCs) (Fig. 3b). Uniform luminal expression of MUC1 demonstrates polarization (Fig. 3b). Cells expressing the ATII markers SFTPC, SFTPB and ABCA3 were present in all structures (Fig. 3b). Airway goblet cells (MUC5B or MUC5AC) were rare while other airway cells (club cells (SCGB3A2), ciliated cells (FOXJ1) and basal cells (KRT5 and P63)) were not detected (not shown). While singly plated LBOs branched randomly in every direction and filled a 6.4mm well within 90 days, they formed branching trees that only occupied a section of the well when plated together in close proximity (Supplementary Fig. 3b). These findings show that branching architecture can be manipulated *in vitro*, and that repulsive interactions between branching structures may play a role in determining their architecture. Mesenchymal cells expressing VIMENTIN and CD90 were present surrounding the structures (Fig. 3b). Their proportion, as determined by flow cytometry for $EPCAM^-$ cells, declined during Matrigel culture to less than 2% of the total population however (Supplementary Fig. 3c). $EPCAM^+$, but not $EPCAM^-$ cells, purified from d25 LBOs yielded branching colonies after plating in Matrigel, albeit with low cloning efficiency (0.30±0.0316%,) (Supplementary Fig. 3d). These branching colonies displayed a similar pattern of marker expression as Matrigel colonies generated from intact LBOs (Supplementary Fig. 3e). These findings indicate that rare progenitors in the LBOs are capable of generating branching colonies, and that mesenchymal cells are not required for branching in these culture conditions.

After >170 days, macroscopic tissue (Fig. 4a) consisting of branching tubules with dilated tips, reminiscent of saccules formed during the saccular stage of lung development, had developed (Fig. 4b, Supplementary Fig. 4a, Supplementary Video 2). 84.86%±5.21% cells were $NKX2.1^+$, while most cells were $SOX9^+$ (76.75±6.89%) and a minority (23.78±5.21%) were $SOX2^+$ (Supplementary Fig. 4b) (n=4, one ESC and three iPS lines). Most luminal cells expressed HT2-280, MUC1, SFTPB, SFTPC and ABCA3 (RUES2 Fig. 4c, iPSCs Supplementary Fig. 4b), identifying these as ATII cells. Electron microscopy showed large numbers of lamellar bodies (LBs), the organelles where surfactant is stored[25] (Fig. 4d, Supplementary Fig. 4c). To examine ATII cell function, we added SFTPB covalently linked to the fluorescent lipid, BODIPY. Within minutes, SFTPB-BODIPY was taken up by the cells and secreted in the lumens (Fig. 4e,f, Supplementary Video 3). Although HOPX, a marker of ATI cells and of putative bipotential alveolar progenitors in the mouse,[20,26] was widely expressed (Supplementary Fig. 4b), other ATI markers (AQP5, CLIC5, AKAP5, CAV1, AGER) were undetectable. SOX9, a marker for the distal tips that is downregulated as alveoli mature and becomes undetectable postnatally, was mostly expressed at the tips and outer edges of the branching structures *in vitro*, consistent with mouse development, where

Author Manuscript Author Manuscript Author Manuscript Author Manuscript

SOX9 is a distal lung marker[27–29] (Supplementary Fig. 4b). Expression of airway markers (MUC5AC, SCGB3A2) in the Matrigel LBO colonies was confined to structures co-expressing SOX2 and SOX9 (Supplementary Fig. 4b), and were therefore likely more proximal. While co-expression of SOX2 and SOX9 is unusual in the mouse[19], numerous larger $SOX2^{+}SOX9^{+}$ structures were identified in the human second trimester fetal distal lung (Supplementary Fig. 4d), suggesting that LBOs recapitulate human lung development. The expression of SOX9, the formation of saccular structures expressing predominantly ATII markers and absence of mature ATI cells are consistent with the canalicular stage of lung development, which occurs at the end of gestation of mice, but during the late second trimester in humans. To further verify the developmental stage of d170 Matrigel LBO cultures, we performed RNAseq on 12 independent samples from RUES2 cells and from three iPSC lines. Cross-referencing with the KeyGenes database, which contains expression profiles of human organs during first and second trimesters of gestation and adulthood[30], showed the best match with second trimester fetal lung, without any match with other organs (Fig. 4g, Supplementary Fig. 4e). Together, the structural, protein expression and transcriptomic data indicate that the d170 Matrigel LBO organoids reached the late second trimester of human gestation.

We next explored whether select infectious and fibrotic lung disease could be recapitulated. We asked whether LBOs infected with respiratory syncytial virus (RSV) display features of human lung infection. RSV is a major cause of lower respiratory tract infection in infants, and causes bronchiolitis with obstruction of small airways[2,31]. There is no licensed vaccine or effective antiviral drug at this time, and immunity after infection is short-lived[32]. RSV tropism in humans includes ciliated cells and alveolar epithelial cells[2,3]. Previous studies in human airway epithelial cell lines showed that cells infected with RSV swell and detach from the epithelium[33], a finding consistent with obstruction of small airways by infected cells in archival pathology specimens and with the clinical syndrome of bronchiolitis[3]. At day 2 after infection of d170 Matrigel LBO cultures with RSV, confocal microscopy revealed shedding of swollen, infected cells into the lumen of the branching structures (Fig. 5a, arrows, Supplementary Video 4). No shedding was seen at day 1, despite evidence of viral infection. RSV infection in LBOs therefore recapitulates important features of infection in humans.

Next, we attempted to model pulmonary fibrosis associated with some forms of Hermansky-Pudlak Syndrome (HPS)[5]. HPS is characterized by pigmentation and bleeding abnormalities caused by abnormal biogenesis and trafficking of lysosome-related organelles (LROs), which include platelet dense granules and melanosomes.[34] Some forms, in particular HPS1, are associated with early-onset and intractable pulmonary fibrosis (HPS interstitial pneumonia (HPSIP)) that is clinically similar Idiopathic pulmonary fibrosis (IPF)[5], is characterized by fibrotic obliteration of alveoli and has a median survival of 3–4 years[35]. The fact that LBs of ATII cells are also LROs[34] potentially explains the association of IPF with some mutations causing HPS[5]. Matrigel colonies derived from LBOs generation from RUES2 cells with CRISPR-CAS9-induced deletion of HPS1 (Supplementary Fig. 5a) exhibited less sharply defined branching structures in Matrigel cultures than the LBOs from parental RUES2 line (Fig. 5b), with an increased fraction of $EPCAM^{-}$ mesenchymal cells (Fig. 5c, Supplementary Fig. 5b), heterogeneously expressing the mesenchymal markers

Author Manuscript Author Manuscript Author Manuscript Author Manuscript

PDGFRA, PDGFRB, SMA, VIMENTIN and CD90 (Fig. 5d, low magnification tile scans in Supplementary Fig. 5c). The $EPCAM^-$, but not the $EPCAM^+$ population, showed strongly enhanced proliferation in cultures of RUES2-HPS1 cells compared to parental cells (Supplementary Fig. 5d,e), indicating that expansion of mesenchymal cells explains the increased fraction of $EPCAM^-$ cells. Surprisingly however, hyperproliferation of $EPCAM^-$ cells was already noticed in RUES2-HPS1 LBOs as early as d15 of suspension culture, prior to detection of any ATII markers. Furthermore, increased hydroxyproline content (Supplementary Fig. 5f) as well as enhanced extracellular matrix (ECM) autofluorescence (Supplementary Fig. 5c) and immunofluorescent staining for collagens 1 and 3 and fibronectin (Fig. 5d, Supplementary Fig. 5g) in RUES2-HPS1 cells indicated increased ECM deposition. Mixing experiments (Supplementary Fig. 5h–j) were consistent with notion that the accumulation of mesenchymal cells was driven by mutant epithelial cells, and not a cell intrinsic property of mutant mesenchymal cells, a finding consistent with the notion that HPSIP[36] and potentially other forms of IPF[4] may be caused by epithelial injury. Together, these findings suggest that it may be possible to model at least some fibrotic pulmonary disease using LBOs.

LBOs and LBO-derived branching colonies in Matrigel *in vitro* and growths after xenografting fulfill the definition of true organoids[1]. Previously reported human lung organoids did not show branching *in vitro* or after xenografting[8,9]. Furthermore, in contrast to LBOs, these were generated in the presence of serum, but in the absence of BMP4, RA and Wnt agonism, which we have shown to be essential for lung specification *in vitro*[10]. Finally these structures did not develop *in vivo* after grafting under the kidney capsule of immunodeficient mice, but required preculture on a bioengineered scaffold to generate airway epithelial cells after subcutaneous transplantation[9].

We could reproduce the morphological features of RSV infection in the distal lung, for which there is currently no model that reproduces human infection. The LBO model also showed evidence of fibrosis in cells lacking HPS1, mutation of which is the most penetrant for a form of pulmonary fibrosis that is clinically, prognostically, radiologically and pathologically indistinguishable from IPF[4,5,36]. It is remarkable, however, that while HPSIP typically arises in the 3rd to 4th decade of life, a fibrotic phenotype could be reproduced *in vitro* within 40 days of directed differentiation. While it cannot be fully excluded that this *in vitro* model in fact reveals a developmental abnormality not observed in patients, it is possible that stress of *in vitro* culture recapitulated the changes induced by senescence and led to the very rapid appearance of the phenotype, in particular since age and telomere dysfunction are prime risk factors for IPF[35,37].

The LBO model has limitations however. After 6 months of culture in Matrigel, the organoids match the second trimester of human gestation in terms of structure, marker expression and genome-wide expression signature. These findings suggest that lung development as modeled in the LBO system keeps pace with human lung development *in utero*. Full, terminal maturation therefore remains a challenge in the organoid field[1]. A second limitation is that branching appears random, a finding consistent with a, as yet unproven, ‘space-filling’ model of branching morphogenesis[38]. However, branching could be directed by plating several LBOs in close proximity to each other in Matrigel, in which

Author Manuscript Author Manuscript Author Manuscript Author Manuscript

case the organoids branch away from each other, suggesting that branching can be manipulated *in vitro*. A third limitation is that the exact nature and patterning of the mesenchyme present in the LBOs is unclear. *In vivo* xenografting revealed that LBO-associated mesodermal cells do not have the potential to generate endothelial cells, bone or skeletal muscle, suggesting that the mesenchyme is specified to some extent. The various mesenchymal lineages in the lung and their ontogeny are still poorly characterized.[6] Pulmonary vasculature is likely not derived from pulmonary mesenchyme however. Proximal pulmonary vessels are derived from a common cardiopulmonary mesenchymal progenitor, while the development origin of the alveolar capillary network likely arises from VE-cadherin^{+} progenitors arising in preexisting trunk vessels.[6,39] A fourth limitation is that the *in vitro* cultures are strongly biased towards distal lung, and, although some areas co-expressing SOX2 and SOX9 expressed more proximal markers for goblet cells and club cell precursors, mature club cells, ciliated cells or basal cells were not observed. We could also not achieve induction of ATI markers *in vitro*, although ATI potential is present after engraftment *in vivo*. It is possible that the cultures were not sufficiently mature to allow development of ATI cells. Alternatively, our current culture condition may drive differentiation of distal progenitor towards ATII cells at the expense of ATI cells.

Taken together, this work indicates that, despite certain limitations, LBOs will be a useful tool for the study of human lung development and possibly for lung disease modeling.

METHODS

Reagents

Reagents used are listed in Supplementary Table 1.

Human samples

The use of human fetal tissues procured by the Human Studies Core at Columbia Center for Translational Immunology was approved by the Columbia University Medical Center (CUMC) Human research review committee and the experiments were performed in accordance with the approved protocols.

Media

hPSC maintenance media consisted of DMEM/F12 (1:1) supplemented with 20% knockout serum replacement, 0.1 mM β-mercaptoethanol, Primocin, and 20 ng/ml FGF-2. Serum-free differentiation (SFD) media consisted of IMDM/Ham's F12 (3:1) supplemented with N2, B27, 0.05% bovine serum albumin, 1% penicillin-streptomycin, 50 μg/ml ascorbic acid, 2mM Glutamax, 0.4 μM monothioglycerol and different growth factor cocktails as indicated in Supplementary Table 2.

hPSCs Maintenance

Rockefeller University Embryonic Stem Cell Line 2 (RUES2, NIH approval number NIHhESC-09-0013, Registration number 0013, passage 17–28), Sendai Virus and modified mRNA generated hiPSC lines from healthy human dermal fibroblasts[7,9] (passage 16–25) and IRF7-deficient C12 hiPSC lines[28] were maintained on mouse embryonic fibroblasts

Author Manuscript Author Manuscript Author Manuscript Author Manuscript

(MEFs) plated at 15,000–18,000 cells/cm^2. Cells were cultured in hPSC maintenance media and medium was changed daily. hPSCs were passaged with Accutase/EDTA washed and replated at a dilution of 1:48. Cultures were maintained in a humidified 5% CO_2 atmosphere at 37°C. Lines are karyotyped and verified for Mycoplasma contamination using PCR every 6 months.

Endoderm induction

Induction of endoderm was carried as previous described[9]. Briefly, MEFs were depleted by passaging onto Matrigel for 24 h supplied with hPSC maintenance media and maintained in a humidified 5% CO_2 atmosphere at 37°C. After MEF depletion, primitive streak and embryoid body induction was performed in embryoid bodies/primitive streak formation media (Supplementary Table 2) in low attachment plates for 12–16 h followed by switching to endoderm induction media (Supplementary Table 2) for 36–40 h. Embryoid bodies were fed every day and maintained in a humidified 5% CO_2/5% O_2 atmosphere at 37°C. Endoderm yield was determined by the expression of CXCR4 and c-KIT. For iPS lines, endodermal cells were purified using human CD184 (CXCR4) MicroBead kit. Cells used in all experiments had > 90% endoderm yield.

Anterior foregut endoderm induction

Anterior foregut endoderm was induced as previous described[9]. On day 4, embryoid bodies were dissociated with 0.05% Trypsin/EDTA and plated on fibronectin-coated multiple well plates with a density at 80,000–105,000 cells/cm^2. Cells were incubated in Anteriorization media-1 for 24 h followed by switching to Anteriorization media-2 for another 24 h.

Formation of lung bud organoids

At the end of anterior foregut endoderm induction, cells were treated with Ventralization media (Branching media) for 48 h and three-dimensional clump formation was observed. The clumps were then suspended by gently pipetting around the wells. The suspended clumps are called lung bud organoids (LBOs) hereafter. LBOs were maintained in non-tissue culture treated multiple-well plates submerged in Branching media and were fed every other day until d20–d25.

Branching morphogenesis in Matrigel

The d20-d25 LBOs were embedded in 100% Matrigel in 24-well transwell inserts and incubated in incubator until the Matrigel solidified. Branching media were added to the well, after which the transwell was inserted, branching media added into the transwell insert as well. Media were changed every other day. A step-by-step protocol describing the generation of LBOs and LBO-derived branching colonies in Matrigel can be found at Nature Protocol Exchange[41].

Immunofluorescence staining

LBOs and branching Matrigel cultures were freshly embedded in Optimal Cutting Temperature (OCT). Samples were sectioned between 5–8 μm, and then air dried for 2 hours. The sections were fixed with 4% paraformaldehyde for 20 minutes at room

Author Manuscript Author Manuscript Author Manuscript Author Manuscript

temperature (RT) and washed with DPBS for 5 minutes. The sections were permeabilized with 0.3% Triton X-100/PBS for 30 minutes followed by blocking in 5% donkey serum for 1 hour. Primary antibodies (Supplementary Table 3) were incubated at 4°C overnight. The next day, sections were washed with DPBS 3 × 5 minutes followed by secondary antibody (Supplementary Table 3) incubation for 2 hours at RT, washed 3 × 10 minutes with DPBS then mounted with DAPI contained fluorescent mounting medium. For 3D imaging, D25 LBOs were stained as described above, but were stained as intact organoids.

Isolation of EPCAM$^+$ and EPCAM$^-$ population from LBOs

LBOs were dissociated by 0.05% Trypsin/EDTA. The cells were stained with APC-conjugated EPCAM for 20 minutes at 4°C. EPCAM$^+$ and EPCAM$^-$ cells were isolated by Fluorescence activated cell sorting (FACS) using a BD Influx Cell Sorter (San Jose, CA).

RNAseq

Total RNA from LBOs was purified using Direct-zol™ RNA MicroPrep kit. RNA concentration and RNA integrity number (RIN) were determined using an Agilent microfluidic RNA 6000 Nano Chip kit (Agilent Technologies, Santa Clara, CA) on the 2100 Bioanalyzer (Agilent Technologies, Santa Clara, CA). Those samples with RIN greater than 9 were used for RNAseq. Poly-A-pull-down was used to enrich mRNAs from total RNA samples. Libraries were prepared using Illumina TruSeq RNA prep kit (Illumina, San Diego, CA). Libraries were then sequenced using the Illumina HiSeq2000 (Illumina, San Diego, CA) at the Columbia Genome Center. Samples were multiplexed in each lane, yielding a targeted number of single-end/pair-end 100bp reads for each sample, as a fraction of 180 million reads for the whole lane. RTA (Illumina, San Diego, CA) was used for base calling and bc12fastq (version 1.8.4) for converting BCL to fastq format, coupled with adaptor trimming. Reads were mapped to a reference genome (NCBI/build37.2) using Tophat (version 2.0.4) with 4 mismatches and 10 maximum multiple hits. To tackle the mapping of reads that are from exon-exon junctions, Tophat infers novel exon-exon junctions ab initio, and combines them with junctions from known mRNA sequences as the reference annotation. We estimated the relative abundance of genes and splice isoforms using cufflinks (version 2.0.2) with default settings. We tested for differentially expressed genes under various conditions using DEseq, an R package based on a negative binomial distribution that models the number reads from RNAseq experiments and tests for differential expression.

In situ hybridization

In situ hybridization was performed on frozen sections (5–8 μm) using digoxigenin (DIG)-UTP-labeled SHH riboprobes. Briefly, human adult lung tissue cDNA was used as template to generate SHH PCR products containing either T7 or T3 promoter sequences (Forward: AATTAACCCTCACTAAAGGGACAGCTCGGAAGTCATCAGTT; Reverse: TAATACGACTCACTATAGGGG CCTCTGAGTGGTGGCCATCTT). The PCR products were used as templates to generate SHH riboprobes using T7 MAXIscript kit (Ambion) followed by RNeasy micro kit (Qiagen) to clean up the riboprobes. Different stages of the LBOs freshly embedded in OCT. Samples were sectioned between 5–8 μm followed by fixation with 4% paraformaldehyde for 20 minutes RT. The sections were washed with DEPC-DPBS for 3× 5 minutes and acetylated in acetylation buffer (584 μl of

Author Manuscript Author Manuscript Author Manuscript Author Manuscript

triethanolamine/50 ml of DEPC-H2O/125 μl acetic anhydride) for 10 minutes. Permeabilization was carried in 0.1% Triton X-100/PBS for 30 minutes at RT followed by washed with DEPC-DPBS 3 × 5 minutes. The sections were incubated with hybridization buffer (5% dextran sulfate/4× SSC/50% formamide/1× Denhardt's/5% fish sperm DNA) for at least 2 hours at RT then overnight with 200 ng/ml of DIG-labeled SHH probe in hybridization buffer at 72°C. The next day, sections were incubated with 0.2× SSC pre-warmed to 72°C for 2 hours followed by cool down to RT for 30 minutes. The sections were washed with fresh 0.2× SSC for 5 minutes then PBS for another 5 minutes. The sections were incubated with blocking solution (2% sheep serum/TBST) for 1 hour followed by anti-DIG-AP Ig overnight at 4°C. The sections were washed with TBST 3 × 10 minutes and rinsed in color reaction buffer (100 mM Tris, pH 9.5/0.1% Tween-20/100 mM NaCl/50 mM $MgCl_2$) for 10 minutes. Color was developed by incubating the section with BM-purple.

Mouse kidney capsule transplantation

The NOD.Cg-Prkdc^{scid}.Il2rg^{tm1Wjl}/SzJ (NSG) mice were housed in a specific pathogen-free mouse facility. All the mice used at 10–13 weeks of age and not selected for gender. The experiment was set up to use 5–7 mice per time point. No statistical method was used to predetermine sample size. The experiments were not randomized. Experiments and animal care were performed in accordance with the protocols approved by The Columbia University Institutional Animal Care And Use Committee. One million of d20-d25 LBO cells were mixed with 5 μl Matrigel prior to surgery and implanted under the kidney capsule. Outgrowths were excised, embedded freshly in OCT for immunofluorescence or fixed in 4% paraformaldehyde for paraffin embedding. Histology was analyzed using hematoxylin/eosin staining.

Dot blots

Three microliter of fluid aspirated from the tubular structures of 5 month grafts was deposited onto a nitrocellulose blotting membrane (GE Healthcare Life Sciences). The dot-blot membrane was air-dried for 5 minutes, and blocked in 5% milk/PBS for 1 hour and then probed with the indicated primary antibodies (Supplementary Table 3) overnight at 4°C. HRP-conjugated secondary antibodies was applied to the membranes followed by signal detection with ECL Western Blotting Detection Reagents and exposure to X-ray film.

Imaging

Samples were imaged using motorized Leica DMI6000 B (Leica Microsystems, Buffalo Grove, IL) or DMi8 (Leica Microsystems, Buffalo Grove, IL) inverted microscopes or 2-photon confocal laser scanning microscope Leica TCS SP8 (Leica Microsystems, Buffalo Grove, IL). Macroscopic images (Fig. 3a and Fig. 5a) were taken using iPhone 6 (Model: MG5A2LL/A, Apple, Cupertino, CA).

Quantification of immunofluorescence

Images for each nuclear marker were quantified using ImageJ. Briefly, images were converted to 8-bit images and the threshold was adjusted to correspond with the nuclear stain, which allows for measurement of total area. The total area was analyzed by the

Author Manuscript Author Manuscript Author Manuscript Author Manuscript

"Analyze Particles" function of ImageJ. Percentage of positive cells were calculated by dividing the total area of positive cells over the total area of DAPI. For extracellular matrix quantification, fluorescence intensity was quantified using Leica Application Suite X. The values were normalized to the RUES2 control for each individual experiment before statistical analysis.

Transmission Electron Microscopy

Transmission Electron Microscopy (TEM) was performed at the NYU Langone Medical Center Microscopy Core. LBOs were fixed with 2.5% glutaraldehyde in 0.1M sodium cacodylate buffer (pH7.2) for 2 hours and post-fixed with 1% osmium tetroxide for 1.5 hours at room temperature, then processed in a standard manner and embedded in EMbed 812 (Electron Microscopy Sciences, Hatfield, PA). Semi-thin sections were cut at 1 mm and stained with 1% Toluidine Blue to evaluate the quality of preservation and find the area of interest. Ultrathin sections (60 nm) were cut, mounted on copper grids and stained with uranyl acetate and lead citrate by standard methods. Stained grids were examined under Philips CM-12 electron microscope and photographed with a Gatan (4k ×2.7k) digital camera (Gatan, Inc., Pleasanton, CA).

Generation of RUES2-HPS1 line

The RUES2-HPS1 line was generated at the Stem Cell Core Facility at Columbia University Medical Center. Briefly, RUES2 cells (passage 25) were cultured in six-well plates coated with Matrigel to 70–80% confluence. Cells were electroporated with 7.5 μg of HPS1 guide RNA plasmid plus 2.5 μg of Cas9mCherry per well of a 6-well plate using Nucleofector 4D. Cas9mCherry-derived mCherry was used as a fluorescent marker to sort transfected cells. Twenty-four hours posttransfection, cells were sorted using FACS with a Bio-Rad S3e cell sorter and seeded at ~2,000 cells/6 cm dish on MEF feeders. Colonies were picked 7–10 days post sorting. Genomic DNAs from individual clones were isolated and genotyping was done using HPS1-specific PCR primers (HPS1-F-1 (GTAGAGGCAGCAGATCCAAGAGG) and HPS1-R-1 (GAACAAGGTGGTCCACACA). 420 bp band to be expected). The PCR products were cloned into a plasmid for proper sequence using In-Fusion reaction (Clontech, Mountain View,CA). Sequencing revealed premature stop codons in each allele (Supplementary Fig. 5).

Uptake of SPB-BODIPY in live LBOs and quantification

d170 LBOs were stained with CellMask™ Deep Red Plasma membrane Stain for 10 minutes and washed for 5 times followed by imaging prior loading SPB-BODIPY to obtained background fluorescence levels (0 min). The cultures then were loaded with 20 ng/ml purified human SPB-BODIPY protein (10 ng in total per culture) directly on top of the Matrigel. Images were taken every 2 minutes using a 2-photon confocal laser scanning microscope (Leica TCS SP8) and the fluorescent intensities were quantified using Leica Application Suite X. The background fluorescence values were subtracted from all measurements before statistical analysis.

Author Manuscript Author Manuscript Author Manuscript Author Manuscript

Hydroxyproline content

Hydroxyproline content was measured followed manufacture's protocol (Sigma, MAK008-1KT). Briefly, samples from RUES2 or RUES2-HPS1 cultures were homogenized by tissue glass Teflon dounce homogenizer (10 mg samples in 100 μl of water) and transferred to a pressure-tight vial followed by adding 100 μl of concentrated hydrochloric acid (~ 12M) per 10 mg of sample. The mixtures were hydrolyzed at 120°C for 3 hours. Samples were dried in a 96 well plate at 60°C followed by Chloramine T/Oxidation Buffer Mixture for 5 mins at RT and DMAB reagent for another 90 mins at 60°C. Hydroxyproline content were measured at 560 nm. The same amount of Matrigel was used as control.

Comparative analysis using KeyGenes

RNAseq data obtained from d170 LBOs from RUES2, C12, HDF SV and HDF mRNA lines was compared to different first and second trimesters and adult organs, including the lungs, using KeyGenes. Hierarchical clustering of 12 samples of the d170 LBOs and 75 samples from 19 organs from second trimester was performed using Cluster 3.0 and viewed by TreeView. The 87 classifier genes were calculated by KeyGenes.

Respiratory syncytial virus preparation and infection

Recombinant red fluorescent protein (RFP)-expressing RSV A2 (rrRSV) was generated from the full-length RSV plasmid[1], MP224 by replacing the enhanced green fluorescent protein gene with the wild-type Discosoma RFP gene from pDsRed. For cell maintenance, HEp-2 cells (ATCC no. CCL-23) and Vero cells (ATCC no. CCL-81) were grown in monolayer culture and maintained in DMEM supplemented with 10% fetal calf serum (FCS) and 2 mM L-glutamine in a humidified atmosphere with 5%CO_2 at 37 °C. Viral stocks were prepared in HEp-2 cells (ATCC no. CCL-23). Briefly, HEp-2 cells were grown overnight, washed with OptiMEM, and inoculated with rrRSV. After a 2.5-h adsorption period the cells were incubated for 3 days in DMEM supplemented with 1% FCS. Virus was harvested by one freeze-thaw cycle followed by a clarifying centrifugation at 3,500 r.p.m. and stored at −80 °C. Viral titers were determined by plaque assay in Vero cells using a 2% methyl cellulose overlay, 5% (v/v) formaldehyde fixation, and crystal violet staining (0.015% w/v) at 5 days. For RSV infection of d170 LBOs, 10^7 plaque-forming units (PFU) of RSV in 1 ml was directly added onto each Matrigel culture in wells and incubated for 3 hrs at 37 °C. The RSV inocula were then removed and the cultures were washed with SFD media 5 times for 5 minutes and maintained in branching media. The cultures were collected at indicated time points for whole mount staining using anti-RSV (all antigens) antibody (Meridian Life Science, B65890G). Images were taking using inverted microscopes or 2-photon confocal laser scanning microscope Leica TCS SP8 (Leica Microsystems, Buffalo Grove, IL).

Data Availability

The RNA sequencing data sets that support the findings of this study are available from the Sequence Read Archive (SRA). The SRA accession number for d25 LBOs sequencing is SRP073749 and SRR4295269 for d170 LBOs. All source data supporting the findings of this study are provided in Supplementary Table 4. All other data supporting the findings of this study are available from the corresponding author upon reasonable request.

Author Manuscript Author Manuscript Author Manuscript Author Manuscript

Statistics and Reproducibility

Statistical analysis was done using unpaired two-tailed Student's *t*-test or one-way ANOVA where appropriate using Prism 7. Results were shown mean±s.e.m., p values < 0.05 were considered statistically significant. N-value refers to biologically independent replicates, unless noted otherwise. The investigators were not blinded to allocation during experiments and outcome assessment in animal studies, as no statistics were performed.

Supplementary Material

Refer to Web version on PubMed Central for supplementary material.

Acknowledgments

This work was supported by grant NIH HL120046-01 (HWS), 1U01HL134760-01 (HWS) RO1 AI031971 (AM), and RO1 AI114736 (AM). RUES2-HPS1 cells were generated by the Columbia Stem Cell Core Facility. We thank NYULMC OCS Microscopy core Chris Petzold and Kristen Dancel for their assistance with transmission electron microscopy. We thank Mark Peeples (Ohio State University) for providing the original recombinant RSV. Flow cytometry was performed in the CCTI Flow Cytometry Core, supported in part by the Office of the Director, National Institutes of Health under awards S10RR027050 and S10OD020056.

References

1. Lancaster MA, Knoblich JA. Organogenesis in a dish: modeling development and disease using organoid technologies. Science. 2014; 345:1247125. [PubMed: 25035496]
2. Collins PL, Fearns R, Graham BS. Respiratory syncytial virus: virology, reverse genetics, and pathogenesis of disease. Current topics in microbiology and immunology. 2013; 372:3–38. DOI: 10.1007/978-3-642-38919-1_1 [PubMed: 24362682]
3. Johnson JE, Gonzales RA, Olson SJ, Wright PF, Graham BS. The histopathology of fatal untreated human respiratory syncytial virus infection. Mod Pathol. 2007; 20:108–119. DOI: 10.1038/modpathol.3800725 [PubMed: 17143259]
4. Mulugeta S, Nureki S, Beers MF. Lost after translation: insights from pulmonary surfactant for understanding the role of alveolar epithelial dysfunction and cellular quality control in fibrotic lung disease. American journal of physiology. Lung cellular and molecular physiology. 2015; 309:L507–525. DOI: 10.1152/ajplung.00139.2015 [PubMed: 26186947]
5. Vicary GW, Vergne Y, Santiago-Cornier A, Young LR, Roman J. Pulmonary Fibrosis in Hermansky-Pudlak Syndrome. Ann Am Thorac Soc. 2016
6. Herriges M, Morrisey EE. Lung development: orchestrating the generation and regeneration of a complex organ. Development. 2014; 141:502–513. DOI: 10.1242/dev.098186 [PubMed: 24449833]
7. Morrisey EE, Hogan BL. Preparing for the first breath: genetic and cellular mechanisms in lung development. Dev Cell. 2010; 18:8–23. doi:S1534-5807(09)00527-9 [pii]. DOI: 10.1016/j.devcel.2009.12.010 [PubMed: 20152174]
8. Dye BR, et al. In vitro generation of human pluripotent stem cell derived lung organoids. eLife. 2015; 4
9. Dye BR, et al. A bioengineered niche promotes in vivo engraftment and maturation of pluripotent stem cell derived human lung organoids. eLife. 2016; 5
10. Huang SX, et al. Efficient generation of lung and airway epithelial cells from human pluripotent stem cells. Nature biotechnology. 2014; 32:84–91. DOI: 10.1038/nbt.2754
11. Green MD, et al. Generation of anterior foregut endoderm from human embryonic and induced pluripotent stem cells. Nature biotechnology. 2011; 29:267–272. DOI: 10.1038/nbt.1788
12. Huang SX, et al. The in vitro generation of lung and airway progenitor cells from human pluripotent stem cells. Nature protocols. 2015; 10:413–425. DOI: 10.1038/nprot.2015.023 [PubMed: 25654758]

Author Manuscript Author Manuscript Author Manuscript Author Manuscript

13. Kumar ME, et al. Mesenchymal cells. Defining a mesenchymal progenitor niche at single-cell resolution. Science. 2014; 346:1258810. [PubMed: 25395543]
14. Hrycaj SM, et al. Hox5 Genes Regulate the Wnt2/2b-Bmp4-Signaling Axis during Lung Development. Cell reports. 2015; 12:903–912. DOI: 10.1016/j.celrep.2015.07.020 [PubMed: 26235626]
15. Liu L, et al. Hedgehog signaling in neonatal and adult lung. American journal of respiratory cell and molecular biology. 2013; 48:703–710. DOI: 10.1165/rcmb.2012-0347OC [PubMed: 23371063]
16. Bellusci S, et al. Involvement of Sonic hedgehog (Shh) in mouse embryonic lung growth and morphogenesis. Development. 1997; 124:53–63. [PubMed: 9006067]
17. Pepicelli CV, Lewis PM, McMahon AP. Sonic hedgehog regulates branching morphogenesis in the mammalian lung. Current biology : CB. 1998; 8:1083–1086. [PubMed: 9768363]
18. Que J, et al. Multiple dose-dependent roles for Sox2 in the patterning and differentiation of anterior foregut endoderm. Development. 2007; 134:2521–2531. DOI: 10.1242/dev.003855 [PubMed: 17522155]
19. Alanis DM, Chang DR, Akiyama H, Krasnow MA, Chen J. Two nested developmental waves demarcate a compartment boundary in the mouse lung. Nature communications. 2014; 5:3923.
20. Treutlein B, et al. Reconstructing lineage hierarchies of the distal lung epithelium using single-cell RNA-seq. Nature. 2014; 509:371–375. DOI: 10.1038/nature13173 [PubMed: 24739965]
21. Sakurai J, et al. Differential expression of the glycosylated forms of MUC1 during lung development. Eur J Histochem. 2007; 51:95–102. [PubMed: 17664159]
22. Cutz E, Pan J, Yeger H, Domnik NJ, Fisher JT. Recent advances and contraversies on the role of pulmonary neuroepithelial bodies as airway sensors. Seminars in cell & developmental biology. 2013; 24:40–50. DOI: 10.1016/j.semcdb.2012.09.003 [PubMed: 23022441]
23. Ban N, et al. ABCA3 as a lipid transporter in pulmonary surfactant biogenesis. The Journal of biological chemistry. 2007; 282:9628–9634. DOI: 10.1074/jbc.M611767200 [PubMed: 17267394]
24. Ciancanelli MJ, et al. Life-threatening influenza and impaired interferon amplification in human IRF7 deficiency. Science. 2015
25. Whitsett JA, Wert SE, Weaver TE. Diseases of pulmonary surfactant homeostasis. Annual review of pathology. 2015; 10:371–393. DOI: 10.1146/annurev-pathol-012513-104644
26. Jain R, et al. Plasticity of Hopx(+) type I alveolar cells to regenerate type II cells in the lung. Nature communications. 2015; 6:6727.
27. Liu Y, Hogan BL. Differential gene expression in the distal tip endoderm of the embryonic mouse lung. Gene expression patterns : GEP. 2002; 2:229–233. [PubMed: 12617806]
28. Rockich BE, et al. Sox9 plays multiple roles in the lung epithelium during branching morphogenesis. Proc Natl Acad Sci U S A. 2013; 110:E4456–4464. DOI: 10.1073/pnas.1311847110 [PubMed: 24191021]
29. Perl AK, Kist R, Shan Z, Scherer G, Whitsett JA. Normal lung development and function after Sox9 inactivation in the respiratory epithelium. Genesis. 2005; 41:23–32. DOI: 10.1002/gene.20093 [PubMed: 15645446]
30. Roost MS, et al. KeyGenes, a Tool to Probe Tissue Differentiation Using a Human Fetal Transcriptional Atlas. Stem cell reports. 2015; 4:1112–1124. DOI: 10.1016/j.stemcr.2015.05.002 [PubMed: 26028532]
31. Florin TA, Plint AC, Zorc JJ. Viral bronchiolitis. Lancet. 2016
32. Simoes EA, et al. Challenges and opportunities in developing respiratory syncytial virus therapeutics. The Journal of infectious diseases. 2015; 211(Suppl 1):S1–S20. DOI: 10.1093/infdis/jiu828 [PubMed: 25713060]
33. Liesman RM, et al. RSV-encoded NS2 promotes epithelial cell shedding and distal airway obstruction. J Clin Invest. 2014; 124:2219–2233. DOI: 10.1172/JCI72948 [PubMed: 24713657]
34. Huizing M, Helip-Wooley A, Westbroek W, Gunay-Aygun M, Gahl WA. Disorders of lysosome-related organelle biogenesis: clinical and molecular genetics. Annu Rev Genomics Hum Genet. 2008; 9:359–386. DOI: 10.1146/annurev.genom.9.081307.164303 [PubMed: 18544035]

Author Manuscript Author Manuscript Author Manuscript Author Manuscript

35. Ryu JH, et al. Idiopathic pulmonary fibrosis: evolving concepts. Mayo Clinic proceedings. 2014; 89:1130–1142. DOI: 10.1016/j.mayocp.2014.03.016 [PubMed: 24867394]

36. Young LR, et al. The alveolar epithelium determines susceptibility to lung fibrosis in Hermansky-Pudlak syndrome. Am J Respir Crit Care Med. 2012; 186:1014–1024. DOI: 10.1164/rccm.201207-1206OC [PubMed: 23043085]

37. Armanios M. Telomerase and idiopathic pulmonary fibrosis. Mutation research. 2012; 730:52–58. DOI: 10.1016/j.mrfmmm.2011.10.013 [PubMed: 22079513]

38. Short K, Hodson M, Smyth I. Spatial mapping and quantification of developmental branching morphogenesis. Development. 2013; 140:471–478. DOI: 10.1242/dev.088500 [PubMed: 23193168]

39. Peng T, et al. Coordination of heart and lung co-development by a multipotent cardiopulmonary progenitor. Nature. 2013; 500:589–592. DOI: 10.1038/nature12358 [PubMed: 23873040]

40. Hallak LK, Spillmann D, Collins PL, Peeples ME. Glycosaminoglycan sulfation requirements for respiratory syncytial virus infection. J Virol. 2000; 74:10508–10513. [PubMed: 11044095]

41. Chen, YW., Ahmed, A., Snoeck, HW. Generation of three-dimensional lung bud organoid and its derived branching colonies. Protoc. Exch. 2017. http://dx.doi.org/10.1038/protex.2017.027

Author Manuscript Author Manuscript Author Manuscript Author Manuscript

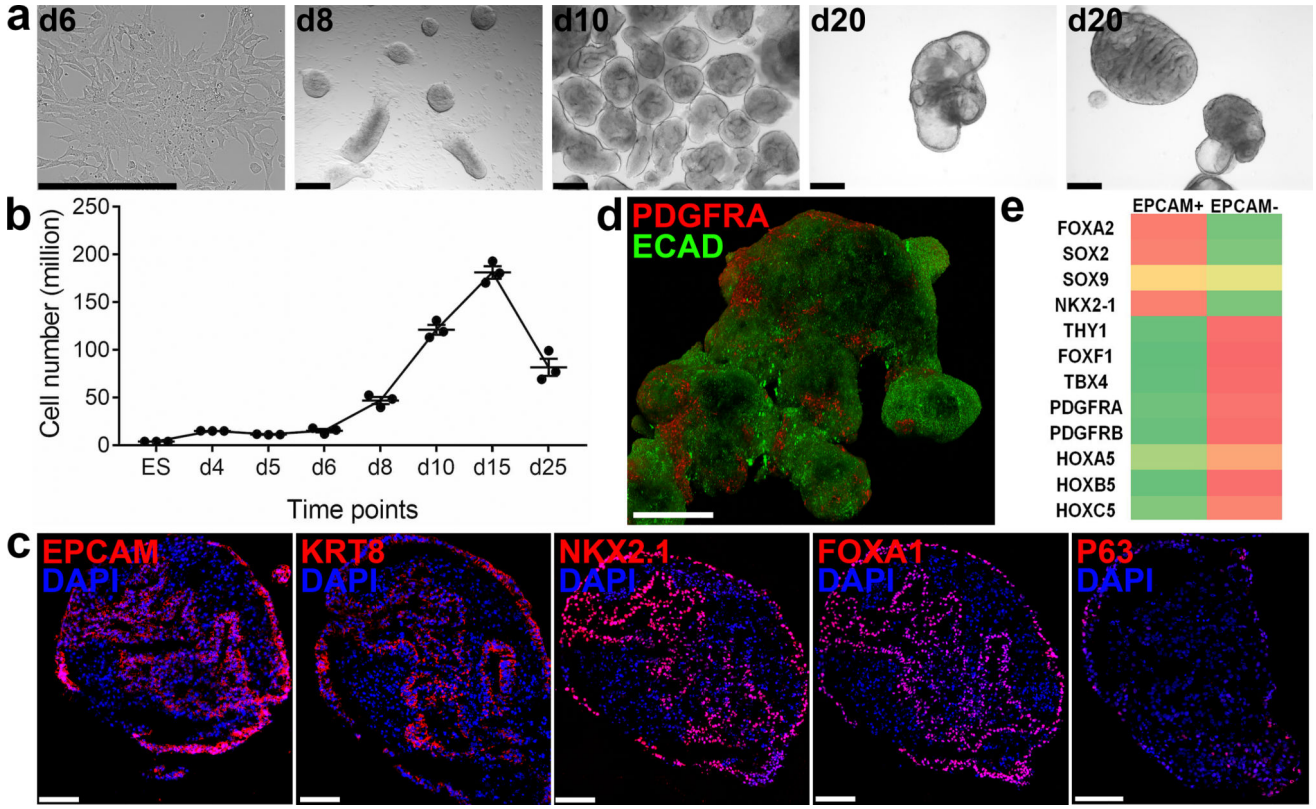

Figure 1. Generation of lung bud organoids

(a) Development of adherent structures during ventralization of AFE between d6 and d8 (see protocol Supplementary Fig. 1b), that could be expanded in suspension culture (d10, d20). Representative of >50 independent experiments (ESCs and iPSCs). Scale bars 250 μm. **(b)** Cellular expansion during the generation of LBOs (mean±s.e.m, n=3 independent experiments in RUES2 ESCs). The source data can be found in Supplementary Table 4. **(c)** Expression of EPCAM, KRT8, NKX2.1, FOXA1, and P63 in d25 LBOs. Representative of >10 independent experiments in ESCs and iPSCs. Scale bars 100 μm. **(d)** Staining of d25 LBO for ECADH and PDGFRA. Representative of 3 independent experiments in RUES2 ESCs. Scale bar 250 μm. **(e)** Expression of endodermal and mesodermal markers in the $EPCAM^{+}$ and $EPCAM^{-}$ fraction of d25 LBOs determined by RNAseq (3 independent biological replicates, RUES2 ESCs).

Author Manuscript Author Manuscript Author Manuscript Author Manuscript

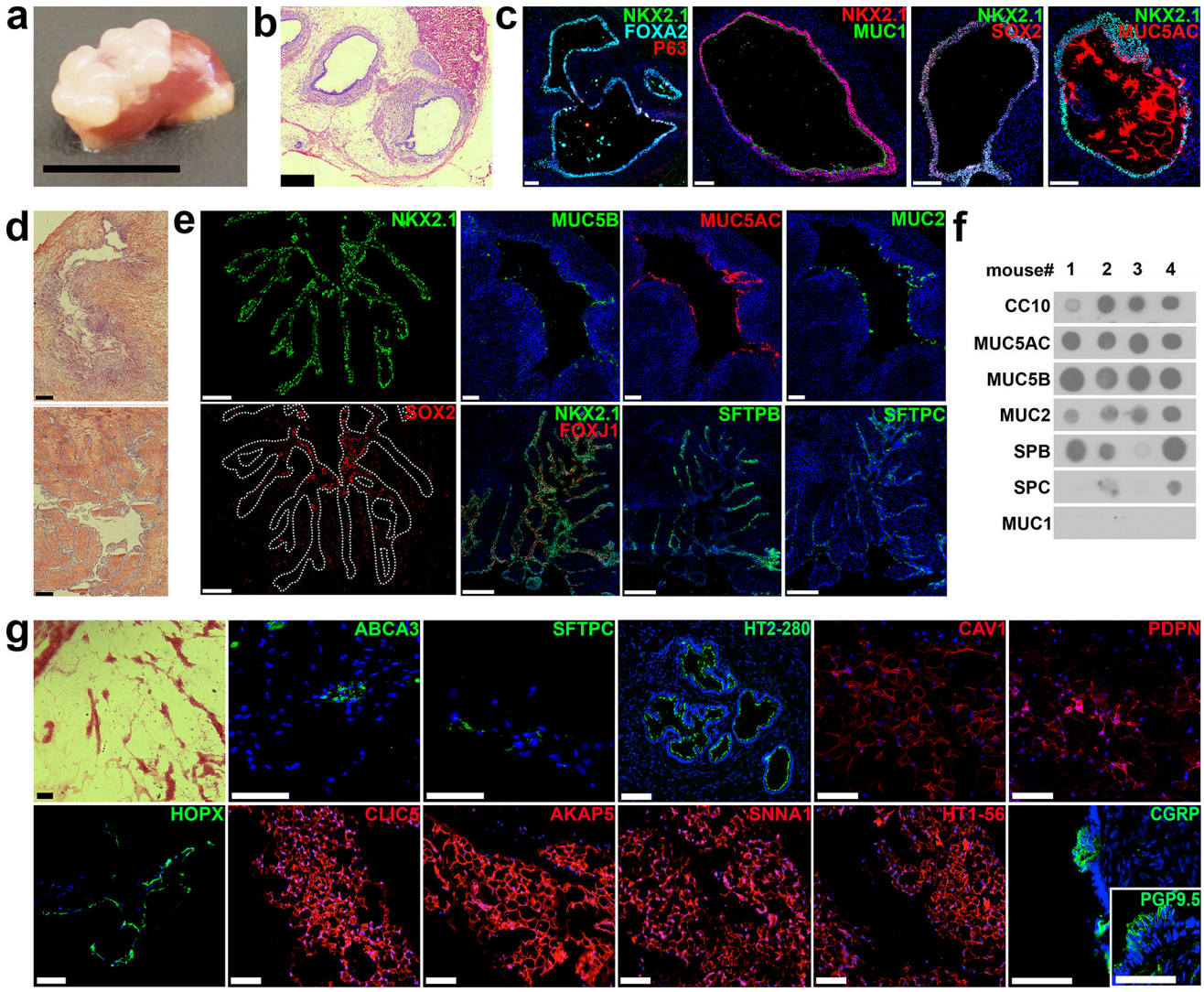

Figure 2. *In vivo* potential of LBOs

(a) Macroscopic aspect of growths 1.5 months after transplantation of 10^6 LBO cells embedded in Matrigel under the kidney capsule of NSG mice. Scale bar 1 cm. **(b)** HE stain of LBO-derived growth 1.5 months after transplantation. Scale bar 500 μm. **(c)** Immunofluorescence for indicated markers in LBO-derived growths 1.5 months after transplantation. Scale bars 100 μm. **(d)** HE staining of LBO-derived growths 5 months after transplantation. Scale bars 250 μm. **(e)** Immunofluorescence for indicated markers in LBO-derived growth 5 months after transplantation. Scale bars 250 μm. **(f)** Dot blots for proteins marked on the left in aspirates from tubules in LBO-derived growth 5 months after transplantation. **(g)** HE staining and immunofluorescence for indicated markers in LBO-derived growths 7 months after transplantation. Scale bars 100 μm. All panels used RUES2 ESCs, representative of 4 independent experiments.

Author Manuscript Author Manuscript Author Manuscript Author Manuscript

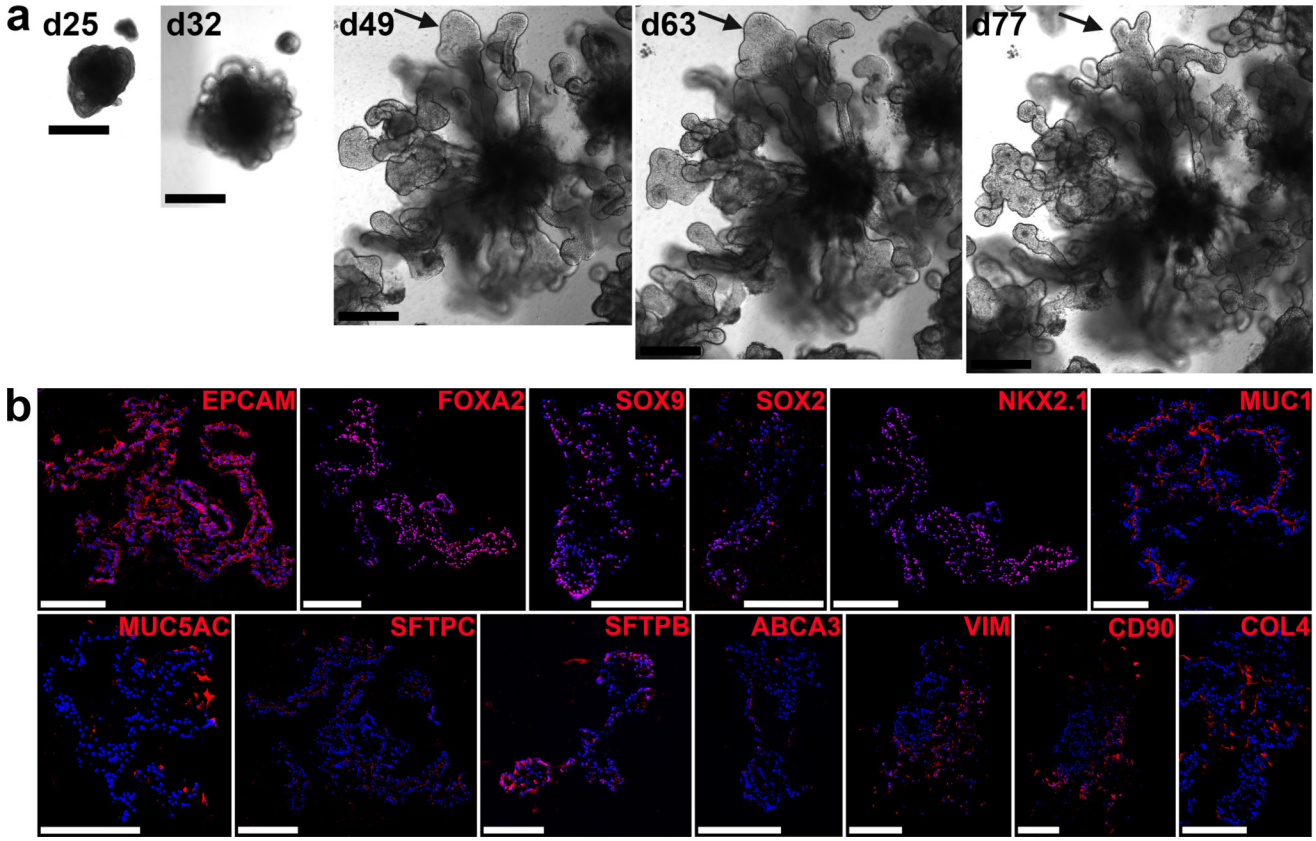

Figure 3. LBO differentiation in Matrigel at d70

(a) Bright field images of the development of an LBO into a branching structure after plating in Matrigel. RUES2 ESCs. Representative of >50 independent experiments. Scale bars 500 μm. **(b)** Immunofluorescence staining for indicated markers in d70 RUES2-derived LBOs plated in Matrigel at d25. Representative of 4 independent experiments. Scale bars 250 μm.

Author Manuscript Author Manuscript Author Manuscript Author Manuscript

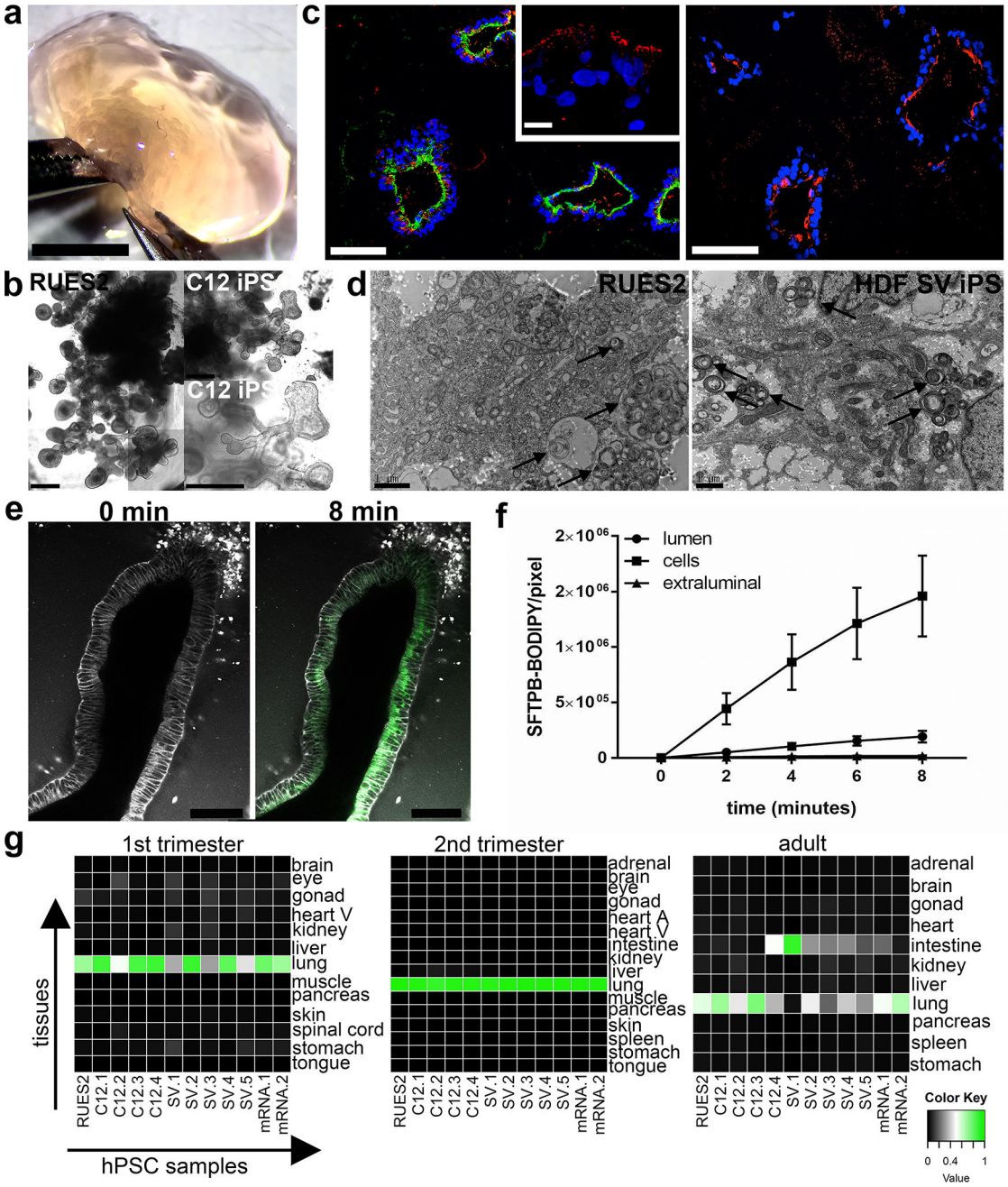

Figure 4. Long-term development of LBOs *in vitro*

(a) Macroscopic appearance of d170 RUES2 LBOs embedded in Matrigel at d25. Representative of >50 independent experiments. Scale bar 5 mm. **(b)** Bright field images of d170 RUES2 and C12 LBOs embedded in Matrigel at d25. Representative of >50 independent experiments. Scale bars 500 μm. **(c)** Immunofluorescence for indicated markers in d170 RUES2 LBOs embedded in Matrigel at d25. Representative of 3 independent experiments. Scale bars for MUC1+SFTPB and HT2-280 100 μm. Scale bar for SFTPC 10 μm. **(d)** Electron microscopy of d170 LBOs embedded in Matrigel at d25 in RUES2 ESCs and HDF SV iPSCs. Arrows indicate LBs. Representative of 3 independent experiments. **(e)**

Author Manuscript Author Manuscript Author Manuscript Author Manuscript

Uptake of SFTPB-BODIPY (green) in d170 LBOs embedded in Matrigel at d25. Representative of 4 independent experiments. Scale bars 100 μm. **(f)** Time-course of uptake of SFTPB-BODIPY in d170 LBOs embedded in Matrigel at d25 (mean±s.e.m, n=4 independent experiments in RUES2 ESCs). The source data can be found in Supplementary Table 4. **(g)** Comparison of genome-wide expression in d170 LBOs derived from hESCs and hiPSCs (12 biologically independent samples) with the KeyGenes database, showing the best match with second trimester human lung.

Author Manuscript Author Manuscript Author Manuscript Author Manuscript

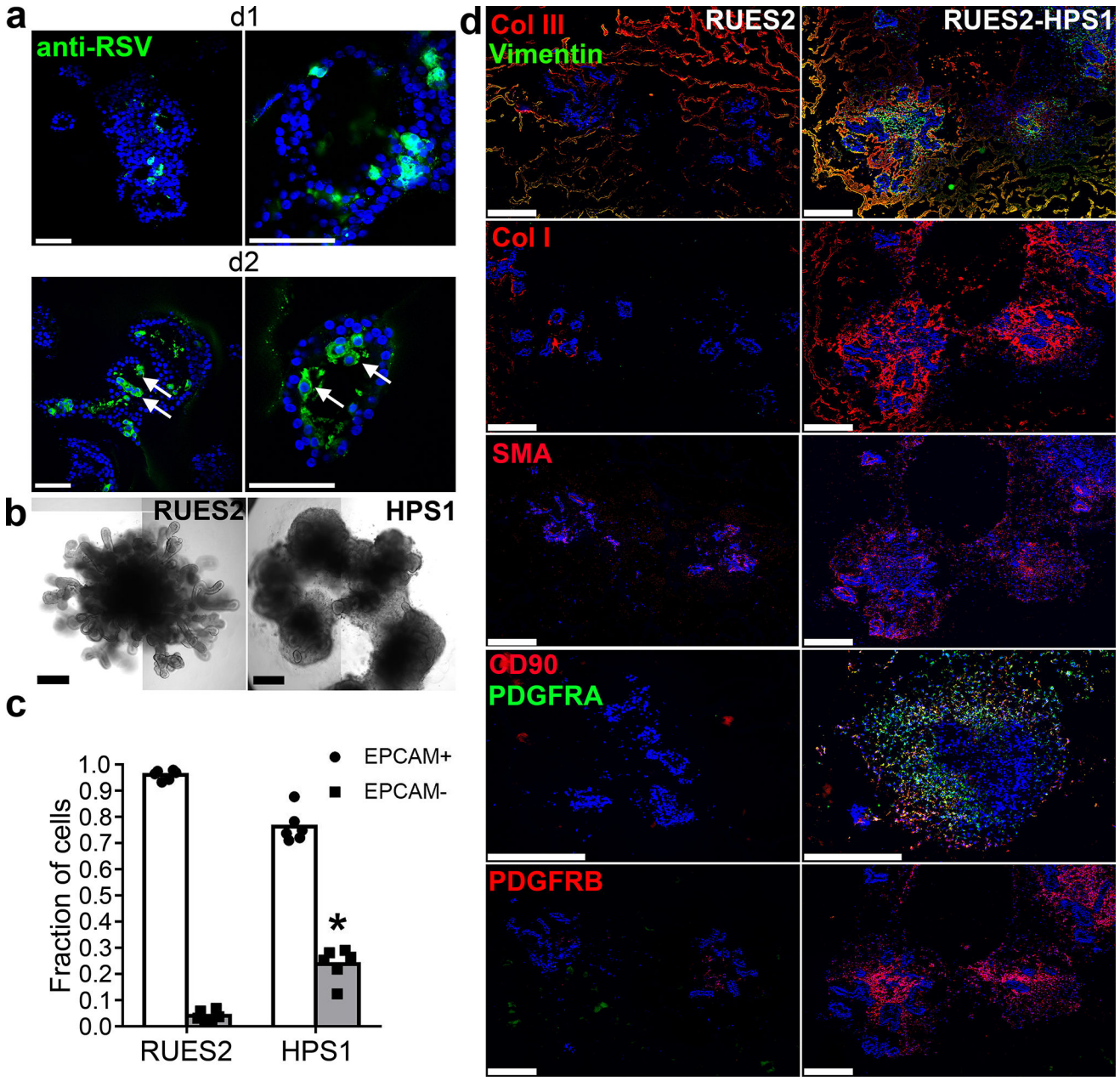

Figure 5. Potential application of LBOs in modeling human diseases

(a) Confocal images of whole mount d170 LBOs 1 and 2 days after infection with RSV and stained using anti-RSV (all antigens) antibody. Arrows: infected cells in the lumen. Representative of 3 independent experiments. Scale bars 100 μm. **(b)** Bright field images of d50 LBO-derived Matrigel colonies from RUES2 and RUES2-HPS1 cells. Representative of six independent experiments. Scale bars 500 μm. **(c)** Fraction of $EPCAM^+$ and $EPCAM^-$ cells in d50 LBO-derived colonies in 3D Matrigel cultures of RUES2 and RUES2-HPS1 cells. (n=6, mean±s.e.m of 3 technical replicates from two experiments; * $P<0.0001$; two-tailed Student's *t*-test). The source data can be found in Supplementary Table 4. **(d)** Immunofluorescence staining for mesenchymal markers and ECM components in 3D

Matrigel cultures of RUES2 and RUES2-HPS1 cells. Representative of 3 independent experiments. Scale bars 500 μm.

Author Manuscript Author Manuscript Author Manuscript Author Manuscript